THE ASTROPHYSICAL JOURNAL SUPPLEMENT SERIES, 148:233–241, 2003 September


# FIRST-YEAR *WILKINSON MICROWAVE ANISOTROPY PROBE* (*WMAP*)[1] OBSERVATIONS: INTERPRETATION OF THE TT AND TE ANGULAR POWER SPECTRUM PEAKS

L. PAGE,[2] M. R. NOLTA,[2] C. BARNES,[2] C. L. BENNETT,[3] M. HALPERN,[4] G. HINSHAW,[3] N. JAROSIK,[2] A. KOGUT,[3] M. LIMON,[3,5] S. S. MEYER,[6] H. V. PEIRIS,[7] D. N. SPERGEL,[7] G. S. TUCKER,[5,8] E. WOLLACK,[3] AND E. L. WRIGHT[9]

*Received 2003 February 11; accepted 2003 May 14*

## ABSTRACT

The CMB has distinct peaks in both its temperature angular power spectrum (TT) and temperature-polarization cross-power spectrum (TE). From the *WMAP* data we find the first peak in the temperature spectrum at $\ell = 220.1 \pm 0.8$ with an amplitude of $74.7 \pm 0.5$ $\mu$K; the first trough at $\ell = 411.7 \pm 3.5$ with an amplitude of $41.0 \pm 0.5$ $\mu$K; and the second peak at $\ell = 546 \pm 10$ with an amplitude of $48.8 \pm 0.9$ $\mu$K. The TE spectrum has an antipeak at $\ell = 137 \pm 9$ with a cross-power of $-35 \pm 9$ $\mu\mathrm{K}^2$, and a peak at $\ell = 329 \pm 19$ with cross-power $105 \pm 18$ $\mu\mathrm{K}^2$. All uncertainties are 1 $\sigma$ and include calibration and beam errors.

An intuition for how the data determine the cosmological parameters may be gained by limiting one's attention to a subset of parameters and their effects on the peak characteristics. We interpret the peaks in the context of a flat adiabatic $\Lambda$CDM model with the goal of showing how the cosmic baryon density, $\Omega_b h^2$, matter density, $\Omega_m h^2$, scalar index, $n_s$, and age of the universe are encoded in their positions and amplitudes. To this end, we introduce a new scaling relation for the TE antipeak-to-peak amplitude ratio and recompute known related scaling relations for the TT spectrum in light of the *WMAP* data. From the scaling relations, we show that *WMAP*'s tight bound on $\Omega_b h^2$ is intimately linked to its robust detection of the first and second peaks of the TT spectrum.

*Subject headings:* cosmic microwave background — cosmological parameters — cosmology: observations — large-scale structure of universe

## 1. INTRODUCTION

*WMAP* has mapped the cosmic microwave background (CMB) temperature anisotropy over the full sky with unprecedented accuracy (Bennett et al. 2003). The temperature angular power spectrum (TT; Hinshaw et al. 2003) and the temperature-polarization cross-power spectrum (TE; Kogut et al. 2003) derived from those maps have a number of characteristic features. It is these features, and our ability to predict them, that make the anisotropy such a powerful tool for cosmology. Computer programs like CMBFAST (Seljak & Zaldarriaga 1996) efficiently compute the TT and TE power spectra for a wide variety of cosmological parameters. The model spectra are then compared with the data to deduce the best-fit parameters (Spergel et al. 2003). The distinctiveness and accuracy of the measured spectrum determines the degree to which the parameters may be distinguished.

While the parameters of cosmological models are ultimately found by maximizing the likelihood of the data given a model, and the validity of a model is assessed by the goodness of fit (Spergel et al. 2003), this analysis by itself provides no model-independent assessment of the features of the angular power spectrum. Both intuition and calculational simplicity fall by the wayside. In this paper we focus on the peaks of the TT and TE spectra. There are four reasons to consider just these particular characteristics. The first is that through an examination of the peaks, one can gain an intuition for how the cosmological parameters are encoded in the TT and TE spectra. The second is that by determining how the peaks depend on cosmological parameters, one may quickly assess how potential systematic errors in the angular power spectra affect some of the cosmological parameters. The third is that alternative models, or additions to the best-fit model, may be easily compared with the data simply by checking to see if the alternative reproduces the peak positions and amplitudes. Finally, the peaks serve as a simple check for the sophisticated parameter fitting described in Spergel et al. (2003) and Verde et al. (2003).

The paper is organized as follows. In § 2 we give a brief overview of the CMB. In § 3 we give *WMAP*'s best-fit values for the positions in $\ell$-space and amplitudes of the peaks. We then consider, in § 4, the cosmological information that comes from the positions and amplitudes of the TT and TE peaks. We interpret the peaks in terms of the best-fit model to the full *WMAP* data set (Spergel et al. 2003) and make direct connections to the decoupling epoch. We conclude in § 5.

## 2. OVERVIEW

The CMB TT spectrum may be divided into three regions depending on the characteristic angular scale of its features. In each region, a different physical process dominates. The regions correspond to (*a*) angular scales larger than the

[1] *WMAP* is the result of a partnership between Princeton University and the NASA Goddard Space Flight Center. Scientific guidance is provided by the *WMAP* Science Team.

[2] Department of Physics, Princeton University, Jadwin Hall, Princeton, NJ 08544; page@princeton.edu.

[3] NASA Goddard Space Flight Center, Code 685, Greenbelt, MD 20771.

[4] Department of Physics and Astronomy, University of British Columbia, Vancouver, BC, V6T 1Z1, Canada.

[5] National Research Council (NRC) Fellow.

[6] Departments of Astrophysics and Physics, EFI, and CfCP, University of Chicago, Chicago, IL 60637.

[7] Department of Astrophysical Sciences, Princeton University, Princeton, NJ 08544.

[8] Department of Physics, Brown University, Providence, RI 02912.

[9] Department of Astronomy, UCLA, P.O. Box 951562, Los Angeles, CA 90095-1562.

TABLE 1
PREVIOUS MEASUREMENTS OF THE FIRST PEAK

| Experiment | $\ell_1^{\rm TT}$ | $\Delta T_{1,\rm TT}$ ($\mu$K) | Cal. Error (%) | $\ell$ Range | Reference |
|---|---|---|---|---|---|
| TOCO | $207^{+15}_{-12}$ | $87^{+9}_{-8}$ | 8 | $60 < \ell < 410$ | Miller et al. 1999 |
| BOOMERANG-NA | $207^{+26}_{-20}$ | $69.6^{+9.7}_{-8.4}$ | 8 | $50 < \ell < 410$ | Mauskopf et al. 2000 |
| MAXIMA | $236 \pm 14$ | $70.0 \pm 5.3$ | 4 | $75 < \ell < 385$ | Lee et al. 2001 |
| DASI | $199^{+15}_{-18}$ | $71.9 \pm 4.4$ | 4 | $110 < \ell < 380$ | Halverson et al. 2002 |
| VSA | $236^{+20}_{-26}$ | $73.9 \pm 6.8$ | 3.5 | $140 < \ell < 420$ | Grainge et al. 2003 |
| BOOMERANG | $219 \pm 5$ | $73.8^{+8.5}_{-7.0}$ | 10 | $100 < \ell < 410$ | Ruhl et al. 2003 |
| ARCHEOPS | $220^{+7}_{-6}$ | $70.2^{+5.7}_{-4.9}$ | 7 | $18 < \ell < 330$ | Benoit et al. 2003 |
| *WMAP* | $220.1 \pm 0.8$ | $74.7 \pm 0.5$ | 0.5 | $100 < \ell < 350$ | This paper |

NOTES.—All values come from fitting a Gaussian shape to just the first peak of the data set specified and include calibration error. Each data set is considered on its own, without the *COBE*/DMR data, and so a direct comparison between experiments may be made. The best-fit position depends somewhat on the fitting function so the values from different analyses yield different results (e.g., Knox & Page 2000; Durrer et al. 2003; Ödman et al. 2002; Grainge et al. 2003). The TOCO, VSA, and BOOMERANG-NA experiments were calibrated with Jupiter. The TOCO and VSA experiments are most affected because of they operate at 30–150 GHz and 35 GHz, respectively. With the new calibration of Jupiter (Page et al. 2003), the peak values above will be reduced ≈5%. The weighted peak amplitude is $71.7 \pm 2.4$ $\mu$K, and the weighted peak position is $218.8 \pm 3.5$, in good agreement with *WMAP*. In a separate analysis based on different assumptions, Bond reports $\ell_1^{\rm TT} = 222 \pm 3$ (J. Bond, 2002, private communication). This was also the value preferred by a concordance model (Wang et al. 2000) that predated all the experiments of the new millennium. Note that *WMAP*'s values for the position and amplitude are both more than 4 times more precise than all the listed measurements combined.

horizon size at decoupling as observed today. These correspond to $\theta > 2°$ or, equivalently $\ell < \ell_{\rm dec} \approx 90$. The low-$\ell$ portion is termed the Sachs-Wolfe plateau (Sachs & Wolfe 1967). In this region one observes the relatively unprocessed primordial fluctuation spectrum because patches of sky with larger separations could not have been in causal contact at decoupling. (*b*) The acoustic peak region, $0.°2 < \theta < 2°$ or $90 < \ell < 900$, which is described by the physics of a 3000 K plasma of number density $n_e \approx 300$ cm$^{-3}$ responding to fluctuations in the gravitational potential produced by the dark matter. (*c*) The Silk damping tail (Silk 1968), $\theta < 0.°2$ or $\ell > 900$, which is produced by diffusion of the photons from the potential fluctuations and the washing out of the net observed fluctuations by the relatively large number of hot and cold regions along the line of sight. The basic framework in which to interpret the temperature anisotropy has been known for over 30 years (Peebles & Yu 1970; Sunyaev & Zeldovich 1970).

It has long been recognized that the positions and amplitudes of the peaks in the $90 < \ell < 900$ region could be used to constrain the cosmological parameters in a particular model (Doroshkevich, Zeldovich, & Sunyaev 1978; Kamionkowski, Spergel, & Sugiyama 1994; Jungman et al. 1996a, 1996b). Previous studies (Scott, Silk, & White 1995; Hancock & Rocha 1997; Knox & Page 2000; Weinberg 2000; Cornish 2001; Podariu et al. 2001; Miller et al. 2002; Ödman et al. 2002; Douspis & Ferreira 2002; de Bernardis et al. 2002; Durrer et al. 2003) have steadily increased our understanding of the peaks and their significance.

A summary of pre-*WMAP* determinations of the position and amplitude of the first peak is given in Table 1.

## 3. DETERMINATION OF PEAK CHARACTERISTICS

We determine the peaks and troughs with fits of Gaussian and parabolic functions to the data. Through this process, we compress a large data set to eight numbers. Such a compression is similar to specifying the cosmological parameters, though it is considerably easier to compute and directed more toward the intrinsic characteristics of the data as opposed to a cosmological model.

For the TT spectrum, $\Delta T_\ell^2 \equiv \ell(\ell+1)C_\ell/(2\pi)$, we model the spectrum for $100 < \ell < 700$ as composed of a Gaussian peak, a parabolic trough, and a second parabolic peak independent of any particular cosmological model. Using a parabola to fit the first peak results in a higher $\chi^2$ and systematically underestimates the amplitude. Parabolas are adequate for the other features. The independent parameters are the amplitude and position of each peak and trough, the width of the first peak, and a continuity parameter. The latera recta[10] of the trough and second peak are derived by constraining the model spectrum to be continuous. The junction between the first peak and the first trough (first trough and second peak) is fixed to be where the first peak (first trough) equals the continuity parameter. In other words, the continuity parameter is the value of the angular power spectrum where the curves meet. There are a total of eight parameters. We denote the positions of the first peak, first trough, and second peak as $\ell_1^{\rm TT}$, $\ell_{1.5}^{\rm TT}$, and $\ell_2^{\rm TT}$, respectively. The amplitudes of the first and second peaks are $\Delta T_{1,\rm TT}^2$ and $\Delta T_{2,\rm TT}^2$.

The peak parameters are found in three ways: (*a*) with a direct nonlinear fit based on the Levenberg-Marquardt algorithm (Press et al. 1992); (*b*) with a Markov chain Monte Carlo (MCMC) (Christensen et al. 2001) of the peak parameters (not the cosmological parameters); and (*c*) with peak-by-peak fits with a Gaussian fitting function. We have also separately fitted the first peak with a Gaussian with additional parameters for kurtosis and skewness. All methods yield consistent results. The values we quote are from the MCMC. All fitting is done with the unbinned angular spectra using the full covariance matrix $\Sigma_{\ell\ell'}$ (Verde et al. 2003). The year 1 *WMAP* calibration uncertainty is 0.5%,

[10] The *latus rectum* of a conic section is the length of the chord parallel to the directix that passes through the focus. For the parabolic curve $y = y_0 + (x - x_0)^2/w$ the value of the latus rectum is $|w|$.

TABLE 2
*WMAP* Peak and Trough Amplitudes and Positions

| Quantity | Symbol | $\ell$ | $\Delta T_\ell$ ($\mu$K) | $\Delta T_\ell^2$ ($\mu$K$^2$) | FULL $\ell$ | FULL $\Delta T_\ell^2$ ($\mu$K$^2$) |
|---|---|---|---|---|---|---|
| First TT peak | $\ell_1^{\rm TT}$ | $220.1 \pm 0.8$ | $74.7 \pm 0.5$ | $5583 \pm 73$ | $219.8 \pm 0.9$ | $5617 \pm 72$ |
| First TT trough | $\ell_{1.5}^{\rm TT}$ | $411.7 \pm 3.5$ | $41.0 \pm 0.5$ | $1679 \pm 43$ | $410.0 \pm 1.6$ | $1647 \pm 33$ |
| Second TT peak | $\ell_2^{\rm TT}$ | $546 \pm 10$ | $48.8 \pm 0.9$ | $2381 \pm 83$ | $535 \pm 2$ | $2523 \pm 49$ |
| First TE antipeak | $\ell_1^{\rm TE}$ | $137 \pm 9$ | ... | $-35 \pm 9$ | $151.2 \pm 1.4$ | $-45 \pm 2$ |
| Second TE peak | $\ell_2^{\rm TE}$ | $329 \pm 19$ | ... | $105 \pm 18$ | $308.5 \pm 1.3$ | $117 \pm 2$ |

Notes.—The values and uncertainties are the maximum and width of the a posteriori distribution of the likelihood assuming a uniform prior. The uncertainties include calibration uncertainty and cosmic variance. The FULL values are derived from the full CMBFAST-based likelihood analysis using just the *WMAP* data (Spergel et al. 2003). The FULL method yields consistent results. Recall that the FULL chains are sensitive to the combined TT and TE spectra and not just the individual peak regions. Numerical errors in CMBFAST will increase the uncertainties but should not bias the results.

which is added in quadrature to the fitted peak amplitude uncertainty. The fit to the TT peak models yields a minimum $\chi^2/\nu = 702/593 = 1.18$. While not as good a fit to the data as a CMBFAST-derived spectrum, the determinations of the peaks are the same for all three methods and are consistent with those of the best-fit CMBFAST model.

For the TE spectrum the data between $40 < \ell < 450$ are modeled as a piecewise-continuous composite of a parabolic antipeak and parabolic peak. (We do not fit the reionization region, $\ell < 20$.) Each parabola has a latus rectum, height, and position; however, the latus rectum of the antipeak is constrained by the requirement that the antipeak and peak are continuously joined at the zero crossing. Thus, there are just five free parameters. We impose a prior on the latus rectum of the peak to be less than 150. The TE Fisher matrix depends on $C_\ell^{\rm TT}$, $C_\ell^{\rm TE}$, and $C_\ell^{\rm EE}$. The TT spectrum is fixed to be a best-fit model, and the small EE contribution is neglected. The best-fit model spectrum has $\chi^2/\nu = 504/466 = 1.08$.

The parameters are summarized in Table 2 along with the peak positions determined directly from the MCMC method. These two completely distinct methods yield consistent results. Figure 1 shows the binned TT and TE angular spectrum with the best-fit peaks model and the 1 $\sigma$ and 2 $\sigma$ contours for the peak and trough positions. The amplitudes of the TT trough and second peak are separated by more than 5 $\sigma$, leaving no doubt of the existence of the second peak.

Also shown in Table 2 are the peak determinations from the full analysis using just the *WMAP* data (Spergel et al. 2003). The agreement between the two is generally good, most of the values are within 1 $\sigma$, and all are within 1.6 $\sigma$. This level of discrepancy is expected because the peak fitting and the full analysis weight the data in very different ways.

## 4. INTERPRETATION OF PEAKS AND TROUGHS

We now interpret the peak characteristics in terms of a flat adiabatic $\Lambda$CDM cosmological model. We focus on the baryon density, $\omega_b = \Omega_b h^2$, the matter density, $\omega_m = \Omega_m h^2$ ($\omega_m = \omega_b + \omega_c$, where $\omega_c$ is the cold dark matter component), and the slope of the primordial power spectrum, $n_s$. The comparison of the peaks and troughs with the model is made at two levels. At the more general level, we use CMBFAST to derive simple scaling relations and show how the cosmological parameters are encoded in the peak characteristics. The aim is to build an intuition for the connection between the raw data and the deduced parameters. This approach has been championed by Hu et al. (2001); this paper forms the basis for our presentation. The scaling relations hold for a wide range of parameters and may be derived without considering *WMAP* data. However, we optimize them for the best-fit *WMAP* parameters (Table 3), so they are as accurate as possible. At a more detailed level, we show that by using the peak values *and* uncertainties with the scaling relations, one obtains constraints and uncertainties on $\omega_b$, $\omega_m$, $n_s$, and the age of the universe that are consistent with the full analysis (Spergel et al. 2003).

Seljak (1994) and Hu & Sugiyama (1995) showed that the physics of the acoustic peaks may be understood in terms of $\omega_b$, $\omega_m$, $n_s$, $\tau$ (the optical depth to when the universe was reionized), and $\theta_A$ (the angular scale of the sound horizon at

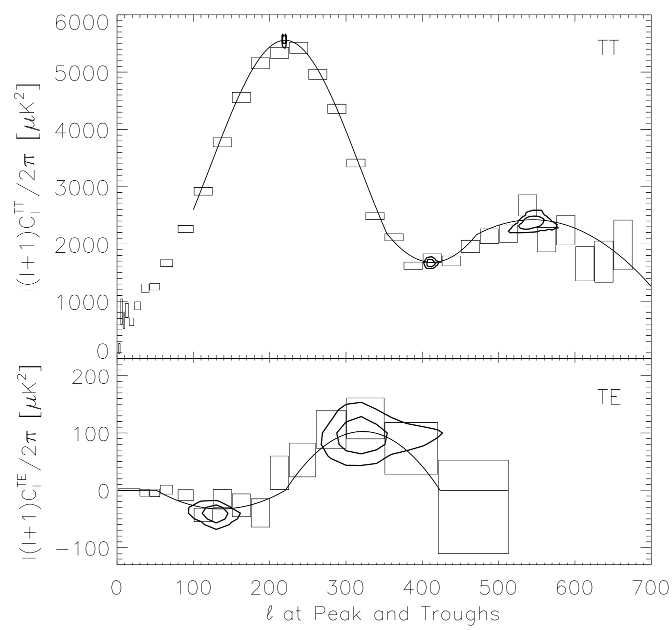


Fig. 1.—Binned *WMAP* data are shown as boxes, the maximum-likelihood peak model from the peak fitting functions is shown as the solid line, and the uncertainties are shown as closed contours. The top panel shows the TT angular power spectrum. The bottom panel shows the TE angular cross-power spectrum. For each peak or trough, the contours from the MCMC chains are multiplied by a uniform prior and so they are equal to contours of the a posteriori likelihood of the data given the model. The contours are drawn at $\Delta\chi^2 = 2.3$ and 6.18 corresponding to 1 $\sigma$ and 2 $\sigma$.

TABLE 3

*WMAP* Cosmological Parameters for the Peaks Analysis

| Quantity | Symbol | Value |
|---|---|---|
| Input | | |
| Physical baryon density | $\omega_b$ | $0.024 \pm 0.001$ |
| Physical mass density | $\omega_m$ | $0.14 \pm 0.02$ |
| Scalar index | $n_s$ | $0.99 \pm 0.04$ |
| Derived from Input | | |
| First TT peak phase shift | $\phi_1$ | $0.265 \pm 0.006$ |
| First TT trough phase shift | $\phi_{1.5}$ | $0.133 \pm 0.007$ |
| Second TT peak phase shift | $\phi_2$ | $0.219 \pm 0.008$ |
| Third TT peak phase shift | $\phi_3$ | $0.299 \pm 0.005$ |
| Redshift at decoupling | $z_{\rm dec}$ | $1088^{+1}_{-2}$ |
| Redshift at matter radiation equality | $z_{\rm eq}$ | $3213^{+339}_{-328}$ |
| Comoving acoustic horizon size at decoupling (Mpc) | $r_s$ | $143 \pm 4$ |
| Derived from Input + Peaks | | |
| Acoustic scale | $l_A$ | $300 \pm 3$ |
| Comoving angular size distance to decoupling (Gpc) | $d_A$ | $13.7 \pm 0.4$ |

Notes.—The cosmological parameters in the top section are derived from just the *WMAP* data assuming a flat ΛCDM model (Spergel et al. 2003). The quantities in the middle section are derived from the cosmological parameters in the top section. The quantities in bottom section are calculated using the middle quantities and the measured position of the first peak. The quantity $z_{\rm dec}$ that we use corresponds to the location of the maximum of the visibility function in CMBFAST. The quantity computed using Hu & Sugiyama 1996 corresponds to $\tau(z_{\rm dec}) = 1$ and is $1090 \pm 2$.

decoupling). Our approach follows that of Hu et al. (2001) in that we consider just the positions of the peaks and the ratios of the peak amplitudes. For $\ell > 40$, the peak ratios are insensitive to the intrinsic amplitude of the CMB spectrum and to $\tau$. The free electrons from reionization at $z \sim 20$ (Kogut et al. 2003) scatter CMB photons, thereby reducing the CMB fluctuations by nearly a constant factor for multipoles $\ell > 40$. (The reionization also increases the TT spectrum at $\ell < 20$ due to Doppler shifts of the scatterers.) We therefore consider just $\omega_b$, $\omega_m$, $n_s$, and $\theta_A$ in the context of a flat ΛCDM model.

### 4.1. *The Position of the First Peak*

The acoustic peaks arise from adiabatic compression of the photon-baryon fluid as it falls into preexisting wells in the gravitational potential. These potential wells are initially the result of fluctuations in some primordial field (e.g., the inflation field in inflationary cosmology). The wells are enhanced by the dark matter ($\omega_c$), which is able to cluster following matter-radiation equality ($z_{\rm eq}$, Table 3) because the dark matter, for our purposes, does not scatter off the photons or baryons.

The first peak corresponds to the scale of the mode that has compressed once in the age of the universe at the time that the photons decoupled from the electrons at $z_{\rm dec}$, some $379^{+8}_{-7}$ kyr after the Big Bang (Spergel et al. 2003). The characteristic angular scale of the peaks is set by

$$\theta_A \equiv \frac{r_s(z_{\rm dec})}{d_A(z_{\rm dec})} \; , \tag{1}$$

where $r_s$ is the comoving size of the sound horizon at decoupling and $d_A$ is the comoving angular size distance to the decoupling surface.

The size of the sound horizon may be computed from the properties of a photon-baryon fluid in an expanding universe. At decoupling it is given by (Hu & Sugiyama 1995, B6)

$$r_s(z_{\rm dec}) = 3997\sqrt{\frac{\omega_\gamma}{\omega_m \omega_b}} \ln \frac{\sqrt{1+R_{\rm dec}} + \sqrt{R_{\rm dec}+R_{\rm eq}}}{1+\sqrt{R_{\rm eq}}} \tag{2}$$

in Mpc, where $R(z) = 3\rho_b(z)/4\rho_\gamma(z)$ with $\rho_b$ the baryon density and $\rho_\gamma$ the photon density. The redshift at matter-radiation equality is

$$1 + z_{\rm eq} = \frac{5464\ (\omega_m/0.135)}{(T_{\rm CMB}/2.725)^4 (1+\rho_\nu/\rho_\gamma)} \; . \tag{3}$$

The ratio of neutrinos to photons is $\rho_\nu/\rho_\gamma = 0.6851$ (Hannestad & Madsen 1995). Note that $r_s(z_{\rm dec})$ depends only on the physical densities, $\omega_m$ and $\omega_b$, and not on $h$. (We assume $T_{\rm CMB} = 2.725$ K [Mather et al. 1999] and the number of neutrino species, $N_\nu = 3$.) Also, $r_s$ is independent of the curvature and cosmological constant densities, $\Omega_k$ and $\Omega_\Lambda$, because these are both late acting: at high $z$ the universe evolves as though it is geometrically flat.

The comoving angular size distance[11] to the decoupling surface, $d_A$, for a flat geometry is

$$d_A = \int_0^{z_{\rm dec}} \frac{H_0^{-1}\, dz}{\sqrt{\Omega_r(1+z)^4 + \Omega_m(1+z)^3 + \Omega_\Lambda}} \; , \tag{4}$$

[11] We follow the naming convention of Peebles (1993), 13.29 for $d_A$. Common alternative names include "proper motion distance" (e.g., Weinberg 1972, 14.4.21), "angular diameter distance" (e.g., Efstathiou & Bond 1999), and "transverse comoving distance" (e.g., Hogg 1999).

where $\Omega_r$ is the current radiation density and $\Omega_\Lambda = 1 - \Omega_m - \Omega_r$ (Peebles 1993). Neither $r_s$ nor $d_A$ depend on $n_s$. The picture one has is that of measuring the angular size $\theta_A$ of a physical meter stick of size $r_s$ near the edge of the observable universe with geodesics of the intervening geometry as encoded in $d_A$.

The position in $\ell$-space of the first peak is intimately linked to $\theta_A$. In fact, in the full analysis (Spergel et al. 2003), $\theta_A$ is one of the best determined fit parameters because of its association with the first peak. To make the connection, one defines a characteristic acoustic index, $\ell_A \equiv \pi/\theta_A$. However, $\ell_A$ is not $\ell_1^{\rm TT}$ because the potential wells that drive the compression, leading to the large variance at $\ell_1^{\rm TT}$, are dynamic: they respond to the matter and radiation that falls into them. Additionally, there is no precise physical relation between an angular scale and an associated $\ell$. One calibrates the relation with cosmological models, such as those from CMBFAST, to find a phase factor $\phi_1$ that relates the two (Hu et al. 2001). The general relation for all peaks and troughs is

$$\ell_m^{\rm TT} = \ell_A(m - \phi_m) , \qquad (5)$$

where $m$ labels the peak number ($m = 1$ for the first peak, $m = 1.5$ for the first trough, etc.). For a particular curvature density, $\Omega_k$, the $\phi_m$-values depend weakly on $\omega_b$, and $\omega_m$. For example, near the *WMAP* values, changing $n_s$, $\omega_b$, and $\omega_m$ by 10% changes $\phi_1$ by 4.6%, 0.5%, and 1.1%, respectively. Because the $\phi_m$-values differ by only $\approx$25% between peaks, $\ell_A$ may be thought of as the characteristic scale of the peaks in $\ell$-space. Effectively, the full analysis solves for the phase factors simultaneously with the other parameters.

The considerations above are quite general and involve a good fraction of the quantities that are of interest to cosmologists. We now show how the *WMAP* peak positions are related to, and in some cases determine, these quantities.

The position of the first peak is an essential ingredient of the mixture of properties that make the CMB such a powerful probe of the geometry of the universe (Kamionkowski et al. 1994; Jungman et al. 1996b). However, the position alone does not determine the geometry. With the full TT spectrum, the quantities that *WMAP* measures particularly well, independent of $\Omega_k$, are $\omega_m$ and $\omega_b$ because both these quantities affect the spectrum at early times, before geometric effects shift the spectrum. Even if $\omega_m$ and $\omega_b$ are known, $\Omega_k$ and $\Omega_m$ (through $h$) may be traded off one another to give the same $\theta_A$. This is called the "geometric degeneracy" (Bond, Efstathiou, & Tegmark 1997; Zaldarriaga, Spergel, & Seljak 1997). The degeneracy is broken with prior knowledge of either $h$ or $\Omega_m$ (e.g., Freedman et al. 2001; Bahcall et al. 1999). For *WMAP* if we impose a prior constraint of $h > 0.5$, then $\Omega_k = 0.03 \pm 0.03$; without the prior, $\Omega_k = -0.050^{+0.036}_{-0.039}$ (Spergel et al. 2003). In the following, we take the geometry to be flat and therefore consider the peak positions as a function of $\omega_b$, $n_s$, and $\omega_m$ only.

With known $\omega_b$ and $\omega_m$, the acoustic horizon size $r_s$ is particularly well determined. From equation (2) we find $r_s = 143 \pm 4$ Mpc. When $n_s$ is included, we may in addition determine the phases. From the fits in Doran & Lilley (2002) we obtain $\phi_1 = 0.265 \pm 0.006$. The uncertainty is derived from the uncertainties of $n_s$, $\omega_b$, $\omega_m$, and the quoted accuracy of the fitting function. This combined with the measured position of the first peak at $\ell_1^{\rm TT} = 220.1 \pm 0.8$ gives us an acoustic horizon scale of $\ell_A = 300 \pm 3$. And, from $\ell_A$ we

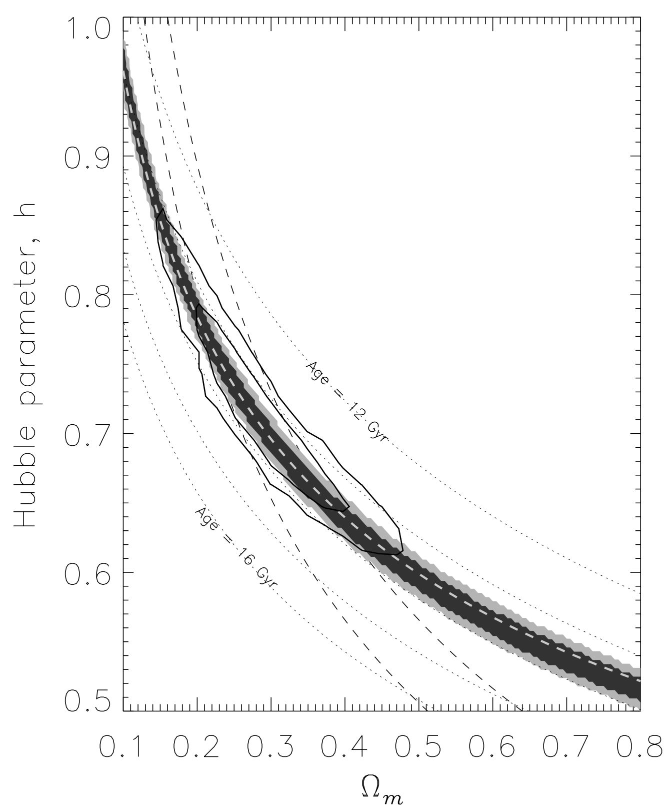


FIG. 2.—*WMAP* data in the $\Omega_m$-$h$ plane. The thick solid contours in black are at $\Delta\chi^2 = -2.3$, $-6.18$ (1 $\sigma$, 2 $\sigma$) of the marginalized likelihood from the full analysis (Spergel et al. 2003). The filled region is the constraint from the position of the first peak, with $\omega_b = 0.023$ fixed. In effect, it shows how $\Omega_m$ and $h$ must be related to match the observed position of the first peak in a flat geometry or, equivalently, to match the measured values of $\theta_A$. The darker inner region corresponds to 1 $\sigma$, and the lighter outer region corresponds to 2 $\sigma$. The dotted lines are isochrons separated by 1 Gyr. It is clear that the *WMAP* data pick out 13.6 Gyr for the age of the universe in the flat, $w = -1$ case. The dashed lines show the 1 $\sigma$ limits on $\omega_m$. The light dashed line shows $\Omega_m h^{3.4}$ = constant.

find that $\theta_A = 0\overset{\circ}{.}601 \pm 0\overset{\circ}{.}005$. In other words, we know the angular and physical sizes of structures on the decoupling surface very well.

From equation (1), we solve for the angular size distance and find that $d_A = 13.7 \pm 0.4$ Gpc. If we had naively tried to compute $d_A$ from $h$ and $\Omega_m$ and their uncertainties directly from equation (4), the resulting uncertainty would have been larger. This, though, is not the correct procedure because the $h$ and $\Omega_m$ deduced from the CMB are correlated as shown in Figure 2.

The interplay between measuring the peak position, and thus $d_A$, and measuring $\omega_m$ is at the root of *WMAP*'s ability to determine $\Omega_m$ and $h$ separately (Bond et al. 1994; Efstathiou & Bond 1999). In particular, Percival et al. (2002) show that $\theta_A$, which depends primarily on the first peak position, is the same along a line of constant $\Omega_m h^{3.4}$. In other words, this is how $\Omega_m$ and $h$ scale to keep $\theta_A$ constant. In Figure 2 we show the constraint from the measured first peak position. For each coordinate pair in the plane, we compute $\ell_1^{\rm TT}$ from equations (1), (2), (4), and (5) and then assign the pair a likelihood derived from the measured distribution of $\ell_1^{\rm TT} = 220.1 \pm 0.8$. (We set $\omega_b = 0.023$ for the calculation as discussed below.) The figure also shows the constraints from $\omega_m$ and the likelihood contours from the full *WMAP* likelihood analysis. It is evident that the departure from a fixed $\Omega_m h^2$ dependence in $\theta_A$ enables separating $\Omega_m$ and $h$. The separation is by no means complete and constitutes one of the largest parameter degeneracies for *WMAP*; it precludes determining $\Omega_\Lambda = 1 - \Omega_m$ to high precision with CMB data alone. The independent determination of $\Omega_m$ and $h$ will improve with time as the uncertainty on $\omega_m$ decreases. Fortunately, galaxy surveys are sensitive to $\Omega_m h$, which breaks the degeneracy when the data sets are combined (Spergel et al. 2003).

It is fortuitous that in a flat geometry the position of the first peak is directly correlated with the age of the universe (Knox, Christensen, & Skordis 2001; Hu et al. 2001). This is seen most easily in the $\Omega_m$-$h$ plane in Figure 2. With $w = -1$, the age depends only on the expansion timescale $h^{-1}$ and $\Omega_m$ and is given by

$$t_0 = 6.52 h^{-1}(1 - \Omega_m)^{-1/2} \ln\left(\frac{1 + \sqrt{1 - \Omega_m}}{\sqrt{\Omega_m}}\right) \text{ [Gyr]} \quad (6)$$

(Carroll, Press, & Turner 1992). We show the isochrons for 12 through 16 Gyr. One observes that they overlap considerably with the position constraint and the degeneracy lines from equation (4).

For reasonable values of $\Omega_m$, the age is seen to be in the neighborhood of 13.6 Gyr. The full analysis (Spergel et al. 2003) gives $t_0 = 13.6 \pm 0.2$ Gyr for $w = -1$. Changing $\omega_b$ changes the position constraint through changes in $r_s$ and $\phi_1$. If $\omega_b$ is increased from 0.024 to 0.025 (1 $\sigma$), the position constraint line shifts by less than $\sigma/2$, indicating that the plot is not particularly sensitive to changes in $\omega_b$.

To summarize this section, we have shown how the position of the first peak is related to the cosmological parameters. Traditionally, one has used equation (5), the weak dependence of $\phi$ on $\omega_b$ and $\omega_m$, $n_s \approx 1$ and the measured position of the first peak to deduce flatness. Instead, we assumed flatness and use *WMAP*'s values of $n_s$, $\omega_b$, and $\omega_m$, to deduce a precise relation for the acoustic scale, $l_A$. We then showed how one of the largest parameter degeneracies in the CMB data could be understood in terms trading off $h$ and $\Omega_m$ in $\theta_A$. Finally, we showed that *WMAP*'s measure of the age of the universe is largely a function of *WMAP*'s identification of the position of the first peak.

### 4.2. *The Amplitude of the First Peak*

The scaling of the amplitude of the first peak with $\omega_b$ and $\omega_m$ has a straightforward interpretation. However, unlike the position, the amplitude itself has a complicated dependence on the cosmological parameters (Efstathiou & Bond 1999; Hu et al. 2001). We defer discussing the $\omega_b$ scaling until after § 4.3 and consider here just the $\omega_m$ scaling.

Increasing $\omega_m$ decreases the first peak height. When the universe is radiation dominated at $z > z_{\rm eq}$ and the photon-baryon fluid compresses in a gravitational potential well, the depth of the well is decreased due to the additional mass loading of the fluid. As a result, the compressed fluid can expand more easily because it sees a shallower potential. The process is termed "radiation driving" (Hu & Sugiyama 1995; Hu & Dodelson 2002) and enhances the oscillations. (In addition, a shallower potential well means that the photons are redshifted less as they climb out, enhancing the effect further.) The effect remains important through recombination. Increasing $\omega_m$, while holding all else but $\Omega_\Lambda$ constant, moves the epoch of matter-radiation equality to higher redshifts without significantly affecting $z_{\rm dec}$. This gives the dark matter more time to develop the potential wells into which the photon-baryon fluid falls. With better defined potential wells, the compressed photon-baryon fluid has less of an effect on them, thereby reducing the effects of radiation driving. As a consequence, increasing $\omega_m$ decreases the amplitude of the fluctuations for all the acoustic peaks.

### 4.3. *Additional TT Peaks and Troughs*

There is a pronounced second peak in the *WMAP* TT spectrum at a height of more than 5 $\sigma$ above the first trough. The peak arises from the rarefaction phase of an acoustic wave. In broad terms (Hu & Dodelson 2002), in the same conformal time that it takes the plasma to compress over the acoustic horizon, an acoustic wave with half the wavelength (twice the $\ell$) of the first peak can compress and rarify. Likewise, a compressional third peak is expected at the second harmonic of the first peak and a rarefaction fourth peak is expected at the third harmonic of the first peak. This set of peaks, the first two of which *WMAP* clearly sees, shows that the photon-baryon fluid underwent acoustic oscillations.

The position of the first trough and the second and subsequent peaks is predicted from the acoustic scale and phase shifts. From equation (5) and the values in Table 3, one predicts $\ell_{1.5}^{\rm TT} = 409 \pm 4$, $\ell_2^{\rm TT} = 533 \pm 5$, and $\ell_3^{\rm TT} = 809 \pm 7$. The first two of these values agree with those found from the peak fits to within the measurement uncertainty as shown in Table 2.

The amplitude of the second peak depends on many of the same parameters as the amplitude of the first. Its most distinctive feature, though, is that increasing $\omega_b$ *decreases* its height. The reason is that as one increases the baryon density one increases the inertia in the photon-baryon fluid. When compared with the lower $\omega_b$ case, the compressions are deeper and the rarefactions not as pronounced. Thus, the compressional peaks are hotter (first and third) and the rarefaction peaks (second and fourth) are cooler.

Following Hu et al. (2001) we characterize the amplitude of second peak as a ratio to the amplitude of the first peak, $H_2^{\rm TT}$. The ratio is insensitive to the reionization optical depth and to the overall amplitude of the spectrum since they simply scale the amplitudes of both peaks. It depends on just $\omega_b$, $\omega_m$, and $n_s$. The dependence on $\omega_m$ is relatively weak, since to a first approximation it too just scales the peak amplitudes as discussed above. The dependence on $n_s$ simply comes from the overall slope of the CMB angular spectrum. Increasing $n_s$ increases the height of the second peak relative to the first. The following function is derived from fitting to a grid of CMBFAST spectra. It gives the ratio of the peak amplitudes to 2% accuracy for 50% variations in the parameters:

$$H_2^{\rm TT} \equiv \left(\frac{\Delta T_2^{\rm TT}}{\Delta T_1^{\rm TT}}\right)^2 = 0.0264 \omega_b^{-0.762} (2.42)^{n_s - 1} \times e^{-0.476 \ln(25.5\omega_b + 1.84\omega_m)^2} ; \quad (7)$$

the parameter dependences are

$$\frac{\Delta H_2^{\rm TT}}{H_2^{\rm TT}} = 0.88 \Delta n_s - 0.67 \frac{\Delta \omega_b}{\omega_b} + 0.039 \frac{\Delta \omega_m}{\omega_m} . \quad (8)$$

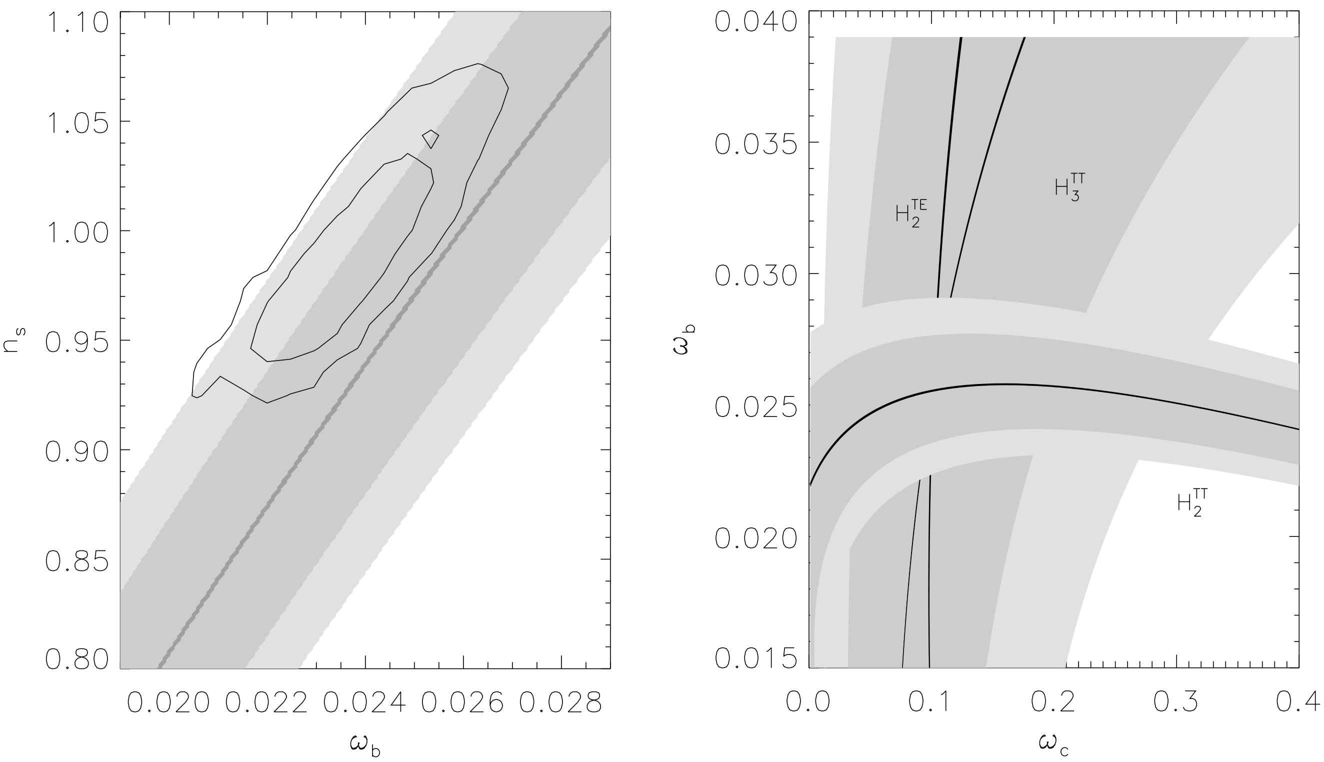


FIG. 3.—*Left*: Parameter restrictions from $H_2^{\rm TT}$ in the $\omega_b$-$n_s$ plane. The gray swath is the 1 $\sigma$ band corresponding to $H_2^{\rm TT} = 0.426 \pm 0.015$ with $\omega_m = 0.14$. The swath is broadened if one includes the uncertainty in $\omega_m$. The light gray swath is 2 $\sigma$. The solid line in the middle of the swath is for $\Delta H_2^{\rm TT} = \Delta\omega_m = 0$. The contours are from the full analysis of just the *WMAP* data and are thus more restrictive. *Right*: The constraints in the $\omega_b$-$\omega_c$ plane from the peak ratios in a flat geometry with $n_s = 0.99$. The darker shaded regions in each swath are the 1 $\sigma$ allowed range; the lighter shaded regions show the 2 $\sigma$ range. The horizontal swath is for $H_2^{\rm TT} = 0.426 \pm 0.015$, and the vertical one is for $H_3^{\rm TT} = 0.42 \pm 0.08$. The leftmost vertical line is for $H_2^{\rm TE} = 0.33 \pm 0.10$. The uncertainty band for $H_2^{\rm TE}$ is not shown as it is broader than the $H_3^{\rm TT}$ swath. The heavier central lines correspond to $\Delta H_2^{\rm TT} = 0$, $\Delta H_3^{\rm TT} = 0$, and $\Delta H_2^{\rm TE} = 0$, each with $\Delta n_s = 0$. As the mission progresses, all uncertainties will shrink.

Thus, a 1% increase in both $\omega_b$ and $\omega_m$ with $n_s$ fixed reduces the height of the second peak relative to the first by 0.63%.

For the *WMAP* data, $H_2^{\rm TT} = 0.426 \pm 0.015$. In Figure 3 we show the constraints from $H_2^{\rm TT}$ for $\omega_m = 0.14$. The contour lines correspond to the full analysis (Spergel et al. 2003). One sees that the two analyses are consistent, though the error from just considering $H_2^{\rm TT}$ is larger. However, it is clear that the uncertainty in $H_2^{\rm TT}$ for $\omega_b$ at fixed $n_s$ and $\omega_m$ leads to nearly the same uncertainty as deduced from the full analysis. Thus, we may interpret *WMAP*'s ability to determine $\omega_b$ as coming primarily from the precise measurement of the ratio of the first two peaks. The first two terms on the right side of the above equation, as shown in Figure 3, also quantify the $\omega_b$-$n_s$ degeneracy (Spergel et al. 2003).

The height of the third peak *increases* as $\omega_b$ increases, as discussed above, and increasing $\omega_m$ decreases its height. Thus, the ratio to the first peak is not as distinctive as for the second peak in terms of $\omega_b$ and $\omega_m$, but the long $\ell$ baseline makes the ratio more sensitive to $n_s$. Hu et al. (2001) give

$$H_3^{\rm TT} \equiv \left(\frac{\Delta T_3^{\rm TT}}{\Delta T_1^{\rm TT}}\right)^2 \tag{9}$$

$$= \frac{2.17\omega_m^{0.59}\ 3.6^{n_s-1}}{[1+(\omega_b/0.044)^2][1+1.63(1-\omega_b/0.071)\omega_m]}\ ,$$

with parameter dependencies

$$\frac{\Delta H_3^{\rm TT}}{H_3^{\rm TT}} = 1.28\Delta n_s - 0.39\frac{\Delta\omega_b}{\omega_b} + 0.46\frac{\Delta\omega_m}{\omega_m}\ . \tag{10}$$

With $n_s$ fixed, increasing $\omega_b$ and $\omega_m$ by 1% increases the height of the third peak relative to the first by only 0.07%. Measuring the third peak helps mostly in measuring $n_s$, thereby breaking the $\omega_b$-$n_s$ degeneracy shown in the left side of Figure 3. For *WMAP* parameters, equation (10) is accurate to 1%.

*WMAP* does not yet clearly measure the third peak. For its height, we use the value of the Wang et al. (2002) compilation because it is the most recent and includes calibration error. At $\ell = 801$, $(\Delta T_\ell^{\rm TT})^2 = 2322 \pm 440\ \mu{\rm K}^2$. Though not quite at the peak, the value is sufficient. With *WMAP*'s first peak, $H_3^{\rm TT} = 0.42 \pm 0.08$.

### 4.4. *The Temperature-Polarization Peaks*

The E-mode polarization in the CMB arises from Thomson scattering of a quadrupolar radiation pattern at the surface of last scattering. At decoupling, the quadrupolar pattern is produced by velocity gradients in the plasma and is correlated with the temperature anisotropy (Bond & Efstathiou 1984; Coulson, Crittenden, & Turok 1994). In rough terms, because it is velocity dependent, the temperature-polarization correlation traces the derivative of the temperature spectrum. For a given TT spectrum, the (nonreionized) TE and EE spectra are predicted. Thus, their observation confirms that the cosmological model is correct but in so far as they are predicted for $\ell > 40$, they contain little additional information about the parameters. By contrast, the TE polarization signal at $\ell < 20$ (Kogut et al. 2003), produced by reionized electrons scattering the local

$z_r \sim 20$ CMB quadrupole, breaks a number of parameter degeneracies and considerably enhances the ability to extract the cosmic parameters.

From parameterizing the output of CMBFAST, we find that the ratio of the first TE antipeak to the second TE peak is given by

$$H_2^{\rm TE} \equiv -\left(\frac{\Delta T_1^{\rm TE}}{\Delta T_2^{\rm TE}}\right)^2 = 0.706\omega_m^{0.349}(0.518)^{n_s-1} \times e^{0.195\ln(33.6\omega_b+5.94\omega_m)^2} . \quad (11)$$

The parameter dependencies are

$$\frac{\Delta H_2^{\rm TE}}{H_2^{\rm TE}} = -0.66\Delta n_s + 0.095\frac{\Delta\omega_b}{\omega_b} + 0.45\frac{\Delta\omega_m}{\omega_m} . \quad (12)$$

The sign preceding $\Delta n_s$ is opposite to that in the case of the TT peaks since we are considering the ratio of the first antipeak (low $\ell$) to the second peak (high $\ell$), whereas in the case of the TT peaks we were considering the second peak (high $\ell$) to the first peak (low $\ell$). Here increasing $\omega_m$ *increases* the contrast between the TE peak and antipeak. This occurs because increasing $\omega_m$ leads to deeper potential wells at decoupling. In turn, this produces higher velocities and thus an enhanced polarization signal. From the data we find $H_2^{\rm TE} = 0.33 \pm 0.10$.

### 4.5. *Combined Peak Constraints*

We now use the scaling relations just presented in a flat model with the scalar index limited to $n_s = 0.99$. This simplified minimal model leads to a greater intuition for assessing the peaks' role in determining the cosmological parameters. The constraints from $H_2^{\rm TT}$ and $H_3^{\rm TT}$ are shown in Figure 3. We see that $H_2^{\rm TT}$ determines $\omega_b$ for most values of the dark matter and that $\omega_b < 0.029$ (2 $\sigma$) regardless of the amount of dark matter. The width of the swath is about twice that of the formal error, again indicating that more in the spectrum than just $H_2^{\rm TT}$ constrains $\omega_b$.

The constraints from $H_2^{\rm TE}$ and $H_3^{\rm TT}$ are almost orthogonal to the $H_2^{\rm TT}$ constraint, but their uncertainty bands are wide. This shows us that the *WMAP* value for $\omega_c$ (or $\omega_m$) is not being driven specifically by the peak ratios. Rather, the constraint comes from the amplitude of the whole spectrum. The degeneracy with $\tau$ is broken by the TE detection of reionization and the degeneracy with the overall amplitude is broken because $\omega_m$ affects primarily the acoustic peak region more than the low $\ell$ part of the spectrum.

## 5. DISCUSSION

We have focused on the dominant acoustic features in the *WMAP* spectrum, but there are other features as well. Notable by its absence is a trough in the TT spectrum at $\ell \approx 10$ due to the increase in fluctuation power near $\ell = 2$ from the integrated Sachs-Wolfe effect in a $\Lambda$-dominated universe. This feature is largely obscured by cosmic variance. For *WMAP* though, there is very little power at low $\ell$ and the correlations with $\theta > 60°$ are unusually small (Bennett et al. 2003a). The lack of even a hint of an upturn at low $\ell$, in the context of $\Lambda$CDM models, is surprising. (However, *COBE* also found no evidence for such an upturn.) This departure from the model constitutes a small (though possibly important) fraction of the total fluctuation power and does not cast doubt on the interpretation of the $\ell > 40$ spectrum.

At $\ell \approx 40$ and $\ell \approx 210$, for example, there are excursions from a smooth spectrum that are somewhat larger than expected statistically. While intriguing, they may result from a combination of cosmic variance, subdominant astrophysical processes, and small effects from approximations made for the year 1 data analysis (Hinshaw et al. 2003). At present, we consider them interesting but do not attach cosmological significance to them (e.g., Peiris et al. 2003; Bose & Grishchuk 2002). More integration time and more detailed analyses are needed to understand how they should be interpreted.

In summary, the characteristics of the peaks of the *WMAP* angular power spectra may be robustly extracted from the data. The second TT peak is seen with high accuracy; the TE antipeak and peak have been observed for the first time. In the context of a flat adiabatic $\Lambda$CDM model, which fits the *WMAP* data well, we report the characteristics of the decoupling surface. By considering a reduced parameter space, we show how the position of the first peak leads to *WMAP*'s tight determination of the age of the universe and how $\omega_b$ is determined primarily from the amplitude ratio of the first to second TT peak. The determination of $\omega_m$ comes from considering the full data set and is not attributable to any particular peak ratio.

L. P. is grateful to Viatcheslav Mukhanov for helpful discussions on the parameter dependences of the peaks during his year at Princeton and to Alessandro Melchiorri for discussing his work on peaks prior to publication. L. P. especially thanks Toby Marriage for many enlightening discussions on the first peak. We also thank Eiichiro Komatsu, Licia Verde, Will Sutherland, and an anonymous reviewer for comments that improved this paper. The *WMAP* mission is made possible by the support of the Office of Space Sciences at NASA Headquarters and by the hard and capable work of scores of scientists, engineers, technicians, machinists, data analysts, budget analysts, managers, administrative staff, and reviewers.

## REFERENCES

Bahcall, N. A., Ostriker, J. P., Perlmutter, S., & Steinhardt, P. J. 1999, Science, 284, 1481
Bennett, C. L., et al. 2003, ApJS, 148, 1
Benoit, A., et al. 2003, A&A, 399, L19
Bond, J. R., Crittenden, R., Davis, R. L., Efstathiou, G., & Steinhardt, P. J. 1994, Phys. Rev. Lett., 72, 13
Bond, J. R., & Efstathiou, G. 1984, ApJ, 285, L45
Bond, J. R., Efstathiou, G., & Tegmark, M. 1997, MNRAS, 291, L33
Bose, S., & Grishchuk, L. P. 2002, Phys. Rev. D, 66, 43529
Carroll, S. M., Press, W. H., & Turner, E. L. 1992, ARA&A, 30, 499
Christensen, N., Meyer, R., Knox, L., & Luey, B. 2001, Classical Quantum Gravity, 18, 2677
Cornish, N. J. 2001, Phys. Rev. D, 63, 27302
Coulson, D., Crittenden, R. G., & Turok, N. G. 1994, Phys. Rev. Lett., 73, 2390
de Bernardis, P., et al. 2002, ApJ, 564, 559
Doran, M., & Lilley, M. 2002, MNRAS, 330, 965
Doroshkevich, A. G., Zeldovich, Y. B., & Sunyaev, R. A. 1978, Soviet Astron., 22, 523
Douspis, M., & Ferreira, P. 2002, Phys. Rev. D, 65, 087302
Durrer, R., Novosyadlyj, B., & Apunevych, S. 2003, ApJ, 583, 33
Efstathiou, G., & Bond, J. R. 1999, MNRAS, 304, 75
Freedman, W. L., et al. 2001, ApJ, 553, 47
Grainge, K., et al. 2003, MNRAS, 341, L23

Halverson, N. W., et al. 2002, ApJ, 568, 38
Hancock, S., & Rocha, G. 1997, in Microwave Background Anisotropies, ed. F. R. Bouchet, R. Gispert, B. Guiderdoni, & J. Tran Tranh Van (Gif-sur-Yvette: Editions Frontières), 179
Hannestad, S., & Madsen, J. 1995, Phys. Rev. D, 52, 1764
Hinshaw, G. F., et al. 2003, ApJS, 148, 135
Hogg, D. W. 1999, Distance Measures in Cosmology (astro-ph/9905116)
Hu, W., & Dodelson, S. 2002, ARA&A, 40, 171
Hu, W., Fukugita, M., Zaldarriaga, M., & Tegmark, M. 2001, ApJ, 549, 669
Hu, W., & Sugiyama, N. 1995, ApJ, 444, 489
———. 1996, ApJ, 471, 542
Jungman, G., Kamionkowski, M., Kosowsky, A., & Spergel, D. N. 1996a, Phys. Rev. D, 54, 1332
———. 1996b, Phys. Rev. Lett., 76, 1007
Kamionkowski, M., Spergel, D. N., & Sugiyama, N. 1994, ApJ, 426, L57
Knox, L., Christensen, N., & Skordis, C. 2001, ApJ, 563, L95
Knox, L., & Page, L. 2000, Phys. Rev. Lett., 85, 1366
Kogut, A., et al. 2003, ApJS, 148, 161
Lee, A. T., et al. 2001, ApJ, 561, L1
Mather, J. C., Fixsen, D. J., Shafer, R. A., Mosier, C., & Wilkinson, D. T. 1999, ApJ, 512, 511
Mauskopf, P. D., et al. 2000, ApJ, 536, L59
Miller, A. D., et al. 1999, ApJ, 524, L1
Miller, C. J., Nichol, R. C., Genovese, C., & Wasserman, L. 2002, ApJ, 565, L67
Ödman, C. J., Melchiorri, A., Hobson, M. P., & Lasenby, A. N. 2002, Phys. Rev. D, 67,83511
Page, L., et al. 2003, ApJ, 585, 566
Peebles, P. J. E. 1993, Principles of Physical Cosmology (Princeton: Princeton Univ. Press)
Peebles, P. J. E., & Yu, J. T. 1970, ApJ, 162, 815
Peiris, H., et al. 2003, ApJS, 148, 213
Percival, W. J., et al. 2002, MNRAS, 337, 1068
Podariu, S., Souradeep, T., Gott, J. R. I., Ratra, B., & Vogeley, M. S. 2001, ApJ, 559, 9
Press, W. H., Teukolsky, S. A., Vetterling, W. T., & Flannery, B. P. 1992, Numerical Recipes in C (2d ed.; Cambridge: Cambridge Univ. Press)
Ruhl, J. E., et al. 2003, ApJ, submitted (astro-ph/0212229)
Sachs, R. K., & Wolfe, A. M. 1967, ApJ, 147, 73
Scott, D., Silk, J., & White, M. 1995, Science, 268, 829
Seljak, U. 1994, ApJ, 435, L87
Seljak, U., & Zaldarriaga, M. 1996, ApJ, 469, 437
Silk, J. 1968, ApJ, 151, 459
Spergel, D. N., et al. 2003, ApJS, 148, 175
Sunyaev, R. A., & Zeldovich, Y. B. 1970, Ap&SS, 7, 3
Verde, L., et al. 2003, ApJS, 148, 195
Wang, L., Caldwell, R. R., Ostriker, J. P., & Steinhardt, P. J. 2000, ApJ, 530, 17
Wang, X., Tegmark, M., Jain, B., & Zaldarriaga, M. 2002, Phys. Rev. D, submitted (astro-ph/0212417)
Weinberg, S. 1972, Gravitation and Cosmology (New York: Wiley)
———. 2000, Phys. Rev. D, 62, 127302
Zaldarriaga, M., Spergel, D. N., & Seljak, U. 1997, ApJ, 488, 1